Available online at www.sciencedirect.com
ScienceDirect
Journal of Magnetic Resonance 188 (2007) 74–82
JMR Journal of Magnetic Resonance
www.elsevier.com/locate/jmr

Operating nanoliter scale NMR microcoils in a 1 tesla field

Andrew F. McDowell [a,*], Natalie L. Adolphi [b]

[a] ABQMR, Inc., 2301 Yale Boulevard SE, Suite C-2, Albuquerque, NM 87106, USA
[b] New Mexico Resonance, 2301 Yale Boulevard SE, Suite C-1, Albuquerque, NM 87106, USA

Received 18 April 2007; revised 15 June 2007
Available online 30 June 2007

Abstract

Microcoil probes enclosing sample volumes of 1.2, 3.3, 7.0, and 81 nanoliters are constructed as nuclear magnetic resonance (NMR) detectors for operation in a 1 tesla permanent magnet. The probes for the three smallest volumes utilize a novel auxiliary tuning inductor for which the design criteria are given. The signal-to-noise ratio (SNR) and line width of water samples are measured. Based on the measured DC resistance of the microcoils, together with the calculated radio frequency (RF) resistance of the tuning inductor, the SNR is calculated and shown to agree with the measured values. The details of the calculations indicate that the auxiliary inductor does not degrade the NMR probe performance. The diameter of the wire used to construct the microcoils is shown to affect the signal line widths.

Keywords: Microcoil; SNR; Permanent magnet

1. Introduction

A variety of experiments in nuclear magnetic resonance (NMR) benefit from the miniaturization of the detector coil. When samples are mass-limited, reducing the detection volume to match the sample size offers enhanced signal-to-noise ratio (SNR) performance, and significant efforts have been undertaken to perfect high-resolution spectroscopy in very small coils [1–9]. The integration of NMR with separation techniques such as liquid chromatography (e.g., [10]) or capillary electrophoresis [11,12] proceeds more naturally when the NMR detection volume can be made compatible with the very small sample volumes and fluid handling tubing typical of the separation step. Researchers have also sought the integration of NMR with microfluidic lab-on-a-chip devices, in which case the NMR detector coil is often formed in a lithographic-type process [13,14]. Very small coils have also been recognized as potential platforms for studying or imaging extremely small objects, even single cells [15–19]. All of the above applications are typically implemented on traditional, high-field superconducting NMR magnets. The small size of a microcoil detector also offers a different opportunity: the miniaturization of the magnet (and indeed the entire NMR apparatus) [20–23] and the application of NMR outside the confines of the traditional NMR research lab. Progress has been made in developing NMR detectors and systems that could find their way onto the factory floor or could be readily transported to where they are needed (e.g., [24,25]).

A fully miniaturized NMR device would be based on a very small permanent magnet. Modern permanent magnet designs [26] result in compact ($<1000\ \mathrm{cm}^3$), lightweight (<10 kg) devices with negligible fringe fields. However, the relatively low-field (1–2 tesla) of the permanent magnet presents a number of challenges. First, the signal-to-noise-ratio (SNR) in NMR is usually proportional to $\omega_0^{7/4} = (\gamma B_0)^{7/4}$, where ω_0 is the NMR frequency and B_0 is the field strength [27]. SNR is already at a premium for micro-scale sample volumes, so detector circuits and electronics must be optimally efficient. Second, at low frequencies the electrical skin depth is no longer small compared to wire diameters, a regime in which optimal NMR SNR performance has not been explored experimentally, to our knowledge. Third, a low field and correspondingly low

* Corresponding author. Fax: +1 505 244 0018.
E-mail address: mcdowell@abqmr.com (A.F. McDowell).

1090-7807/$ - see front matter © 2007 Elsevier Inc. All rights reserved.
doi:10.1016/j.jmr.2007.06.008

NMR frequency presents a new challenge for microcoil developers: the construction of an electrically resonant LC probe circuit from the very-low-inductance sample coil. We have recently proposed and implemented [28] a solution to this problem that introduces a large, fixed-value, auxiliary inductor to eliminate the need for a very large tuning capacitance, which would be awkward to use and would be inconsistent with the design goals of a practical compact system. Understanding and meeting the particular challenges of operating very small NMR detector coils in low-field permanent magnets is a crucial step toward the realization of very small, simple, and inexpensive NMR systems that are capable enough to enable new applications.

Our initial results in the development of such systems [28] indicate that performing NMR using micro-scale coils in compact permanent magnets will be feasible. For a 264 nL sample volume (400 μm diameter, 2.1 mm long cylinder of water) we achieved a single shot SNR of 137 and a line width of 2.5 Hz (56 ppb). However, a number of questions remain after these first measurements. Our first coil was manufactured by a novel but complicated process (focused ion beam milling) which is incompatible with the rapid fabrication of inexpensive sensors. Development of a simpler coil manufacturing technique that achieves high SNR and line width performance is required. Our first coil had a large resistance and hence sub-optimal SNR performance. Improvements in the SNR performance should be made, as these will allow reductions in sample volume and aid further miniaturization. Although our novel tuning circuit produced an adequate signal, we need to confirm that it does not degrade SNR.

In this study, we measure and analyze the performance of a series of very small copper wire-wound coils of various sizes. We describe our methods for constructing the coils and detector circuits, including a method for designing appropriate auxiliary inductors. We demonstrate that the SNR performance of our detectors can be accurately calculated (without adjustable parameters) and that the auxiliary inductors enhance the implementation of microcoil detectors without degrading their performance. We use the quantitative understanding of the SNR performance of our initial set of detectors to discuss the design of an improved detector.

2. Construction methods

2.1. Winding coils

As our goal is to construct small portable NMR systems at reasonable cost, we seek a method for manufacturing microcoils that is significantly simpler than the focused ion beam techniques used to construct the coil for our first experiments. The classic coil construction method is "hand-winding" using standard (usually enameled) wires. A simple gear-synchronized device for accurately winding very small coils on pulled pipette tips has been previously described [17]. The main requirements of any such device are methods for holding the sample tube and rotating it and for controlling the position of the very fine wire as it is taken up on the tube. We find that these requirements are readily met through the use of a miniature lathe [Micro Lathe II, Taig Tools, Chandler, AZ] in conjunction with optical fiber chucks [Newport, FPH-S and FPH-J] appropriately sized to hold micro-capillary tubes [Vitrocom, e.g., CV1017]. The tube is mounted to the headstock of the lathe using the fiber chuck. One end of the wire is taped to the fiber chuck while the other is taped to a support whose position is controlled by the saddle and cross-feed of the lathe. A 7× to 30× dissecting microscope is used to visually monitor the coils as they are wound by gradually turning the headstock and repositioning the cross-feed of the lathe by hand. The capillary tubes are very flexible, and their deflection while winding aids in maintaining the proper tension on the wires [typically 50 gauge enameled copper, California Fine Wire]. When finished, the coil is secured to the tube using standard five-minute epoxy (Locktite "Quick Set"). With minimal practice, coils can be wound in about 15 min.

The key to this rapid coil construction lies in our choice to close-wind our coils. Generally, NMR practitioners assume that coils should be wound with some space between the turns [27,29] in order to avoid strong proximity effects that can increase the high-frequency resistance of the coil windings, leading to excess electrical noise. However, we are operating our coils at rather low frequencies, low enough that the diameter of our wire is only about 2.5× larger than the radio frequency (RF) skin depth. Furthermore, the enamel layer on our wire is about 6 μm thick, yielding a measured 37 μm turn-to-turn spacing. (The diameter of 50 gauge bare copper wire is 25 μm.) Under these conditions, the RF resistance is enhanced over the DC resistance by 4% due to the skin effect and only an additional 4–11% due to the proximity effect [1]. On the other hand, a close-wound coil has the highest possible pitch and hence the highest signal detection sensitivity. The high performance of close-wound microcoils has been demonstrated experimentally [17]; the SNR was found to be maximal for minimal turn spacing. The practical benefit of close winding is that it greatly reduces the need to accurately control the wire during coil construction.

We chose our coil lengths to match the tube inner diameter (except for the largest coil) so that the sample volume aspect ratio is close to unity. This choice is guided by our goal of detecting single magnetic beads [28]. The ratio of outer to inner diameter is very similar for the smaller capillary tubes, so that the coils wound on these tubes and the sample spaces are essentially equivalent up to an overall scale factor.

2.2. Designing the probe circuit

In our earlier work with microcoils, we introduced the counterintuitive idea of using a large, fixed-value auxiliary

inductor in the resonant circuit of the probe. While not strictly necessary for the "large" (550 μm diameter) coil in our earlier work, such an auxiliary inductor is a practical necessity for smaller coils operating at low frequency. There are at least two benefits of the auxiliary inductor. Very small sample coils cannot be resonated at the low operating frequencies typical of permanent magnet based NMR devices without the use of very high capacitances. Either a physically large variable capacitor (contrary to the goal of miniaturization) or a large amount of fixed capacitance in parallel with a variable capacitor (which reduces the tuning range, awkward given the field drifts of permanent magnets) would be required. Furthermore, it is difficult to construct a resonant circuit for a microcoil without introducing paths for circulating currents whose inductances are larger than the branch of the circuit that contains the microcoil. This is especially true for circuits that contain more than one tuning capacitor in parallel. Under such conditions, the circuit as a whole may well resonate at the desired frequency, but the current paths in this resonant mode will largely avoid the branch of the circuit containing the sample coil. An auxiliary inductor, placed in series with the microcoil, both forces the resonant current to flow through the sample coil and reduces the need to include numerous capacitors and their multiple, competing current paths.

The auxiliary inductor raises the Q of the probe circuit. For high-resistance microcoils, the resulting Q is still modest (~10–20), rendering the electrical resonance easy to detect without presenting difficulties with respect to probe stability or excessive ring-down. As we show below, the presence of the tuning inductor does not influence the SNR performance of the NMR detector. Q is changed without altering SNR, highlighting the fact that Q is not a fundamental figure of merit for NMR detection circuits.

Proper design of the auxiliary inductor insures that it does not degrade the SNR performance of the probe over what theoretically could be achieved without the auxiliary inductor. The key idea is that the auxiliary inductor should not contribute to the resistance of the resonant circuit. It is stray *resistance* that degrades the performance of NMR circuits, not stray *inductance* [29]. Once the microcoil has been wound, its RF resistance can be measured or calculated, and this value serves as the starting point for auxiliary inductor design. Ideally, the RF resistance of the auxiliary inductor should be much less than that of the microcoil. If the inductor adds 10% to the circuit's RF resistance, the SNR will be reduced by 5%. To minimize its resistance, the auxiliary inductor is wound using large diameter wire. For our probes, we typically choose 14 gauge copper wire (diameter = 1.63 mm). Given that the current will be carried only at the outer surface of the wire, we can calculate the longest piece of such wire ($=l_{\text{wire}}$) consistent with our goal of low resistance. Starting from the standard approximation for the inductance of a coil of n turns [27]:

$$L = \frac{n^2 r_{\text{coil}}^2}{25 l_{\text{coil}} + 23 r_{\text{coil}}} \tag{1}$$

and substituting the approximate expressions $l_{\text{coil}} \cong n k d_{\text{wire}}$ (d_{wire} is the diameter of the wire, and k is usually 1.3 so that there is a gap from turn to turn) and $n \cong l_{\text{wire}}/(2\pi r_{\text{coil}})$, one can show that the maximum inductance that can be constructed from a wire of length l_{wire} is achieved with a coil of radius:

$$r_{\text{coil}} = \sqrt{\frac{25 l_{\text{wire}} k d_{\text{wire}}}{46\pi}}. \tag{2}$$

Our microcoils have RF resistances that are typically 0.2–1.0 Ω at our operating frequency (44 MHz), and the calculated auxiliary inductors are conveniently sized (radius 0.3–0.6 cm, 2–4 turns).

With the auxiliary inductor properly constructed, we build the remainder of our NMR probe circuit using very simple techniques. A small rectangle of acrylic sheet (roughly $4 \times 3 \times 0.7$ cm) serves as a mechanical support. Small pieces of adhesive-backed copper foil are cut and placed on the acrylic block so that the sample coil, auxiliary inductor, and tuning and matching capacitors can all be mounted on the block. The capillary tube on which the sample coil is wound is glued into two lengths of flexible tubing (we have used PEEK and Radel) using standard five-minute epoxy. This structure is in turn glued to the acrylic block so that the fragile capillary tube is isolated from mechanical shocks transmitted along the flexible tubing. The auxiliary inductor and capacitors (Murata Electronics, TZ03 series) are soldered to the copper foil, and the acrylic-block-mounted module is then installed in a shielded probe body (we have used cast aluminum boxes, or plastic boxes covered with copper foil). A photograph of one of the detector modules is shown in Fig. 1. As we show below, these very simple and crude probe construction techniques yield NMR detectors that achieve optimal performance.

3. Results

Using the methods described above, we have wound a series of microcoils of different sizes, as detailed in Table 1. All of these coils were wound with 50 gauge wire. We designate the capillary size with two numbers, the outer diameter and inner diameter of the tube, in micrometers. The length of the coil is calculated from the number of turns and measured total wire diameter of 37 μm. The sample volume is calculated from the tube inner diameter and the coil length. The inductance is calculated using Eq. (1). The three smallest coils were built into probe circuits that contained an auxiliary inductor: three turns of 14 gauge bare copper wire with a 14.5 mm diameter (calculated inductance 150 nH). The probe circuit for the largest coil did not employ an auxiliary inductor.

To determine the SNR, we performed a single-pulse experiment and acquired a single two-channel free induction decay (FID) signal. For all of our experiments, we

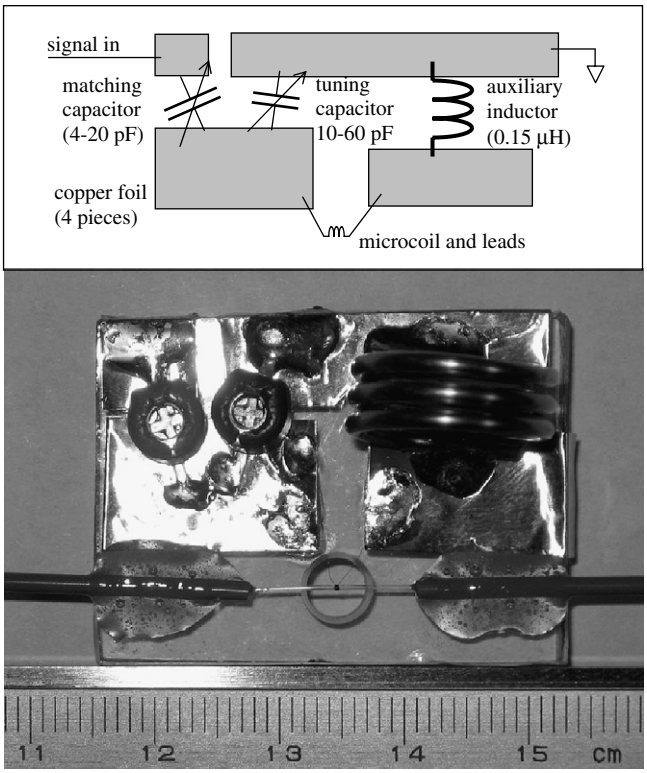

Fig. 1. The microcoil probe module. The top panel is a schematic arranged in the same way as the actual circuit. The bottom panel shows the circuit as mounted on an acrylic block. The microcoil itself is in the lower middle of the picture, centered over a round hole in the acrylic. The capillary tube (330 μm OD, 200 μm ID) is glued into the two sections of flexible tubing which exit the picture to the right and left, and are glued to the acrylic block. The three turn auxiliary inductor is at the upper right. The two round objects with crosses at their centers are the matching and tuning capacitors, respectively.

used a 1.04 tesla permanent magnet with a 5 cm clear gap equipped with linear gradient/shim coils. This is hardly a portable magnet; however it has the same field as our 0.6 kg 1 tesla magnet, and the much larger gap facilitates rapid detector prototyping. The NMR console was a compact imaging system from MR Technology (Japan). The pre-amp (Digital Signal Technology, Japan, model LNA1-42.58M) has a noise figure specified as <1.5 dB and a 50 dB gain. The sample fluid was Magnevist(Gd)-doped water ($T_1 \sim 430$ ms) delivered by syringe though the tubing attached to the capillary. To determine the SNR, the detected signal was corrected for baseline offset and then mathematically adjusted to be on resonance with all of the signal power in one of the channels. The resulting "on-resonance" FIDs are shown in Fig. 2. The noise value was taken to be the standard deviation of the data in the baseline region, the last 50% or so of the data set. The signal was determined by extrapolating the FID back to zero time. Extrapolation was necessary because our narrow bandwidth filters ring for a significant time after the RF pulse. (Our console, designed for imaging, is not optimized for operation at our narrow bandwidths and is not equipped with a adjustable receiver muting circuit.) The measured SNR values are given in Table 2 and have an estimated uncertainty of 10%, which comes from both the extrapolation and from the uncertainty in the standard deviation of the baseline data. When empty of fluid, the coils generated no detectable NMR signal.

We calibrated the overall spectrometer gain by driving the transmit/receive switch input of the console with a −130 dBm signal from a HP8640B RF source. The noise we detect from our probe corresponded to −145.3 dBm at the input to the console, 1.7 dB above the expected thermal noise from a 50 Ω resistor at room temperature (in a band width of 500 Hz). We attribute the 1.7 dB of excess noise to our preamp; our noise measurements are therefore 20% higher than the noise actually produced by our probe. We have multiplied our measured SNR values by 1.2 to correct for this excess noise.

The minimum achieved line width (FWHM of a Lorentzian fit to the Fourier Transform of FID data) is also given in Table 2. The probe was carefully positioned in the most homogeneous location in the magnet, and the linear shims were adjusted to maximize the lifetime of the FID (and optimize its shape). The shims typically provided a 2–5-fold reduction in the line width. The line widths reported in Table 2 are the narrowest we achieved, and the resonance peaks are displayed in Fig. 3. Typically, careful placement of each probe into the same position in the magnet allowed the line width to be reproduced to within 20%. The FID data were time shifted by 28, 10, 10, and 6 ms (smallest coil to largest) in order to avoid distortions due to filter ringing. Transforming without the time shifts gave the same line width values; the lines are well-fit by Lorentzian peaks. Deionized water was used as the sample fluid to avoid lifetime broadening. Hence, the FID data used to determine minimum line widths were not the same as those used to determine maximum SNR.

The DC resistance of the microcoils, given in Table 2, was measured with a benchtop DMM (Fluke 8840 A/AF) operating in two-wire mode. The resistance of the microcoil together with the leads connecting it to the rest of the probe circuit was measured. The DMM lead resistance of 0.040 ± 0.005 Ω was subtracted from the measured values,

Table 1
Microcoil probe parameters

Capillary OD/ID (μm)	Turns	Length (μm)	Calculated inductance (nH)	Sample diameter (μm)	Sample volume (nL)
170/100	4	148	3	100	1.2
250/150	5	185	7	150	3.3
330/200	6	222	13	200	7.0
550/400	17.5	648	120	400	81

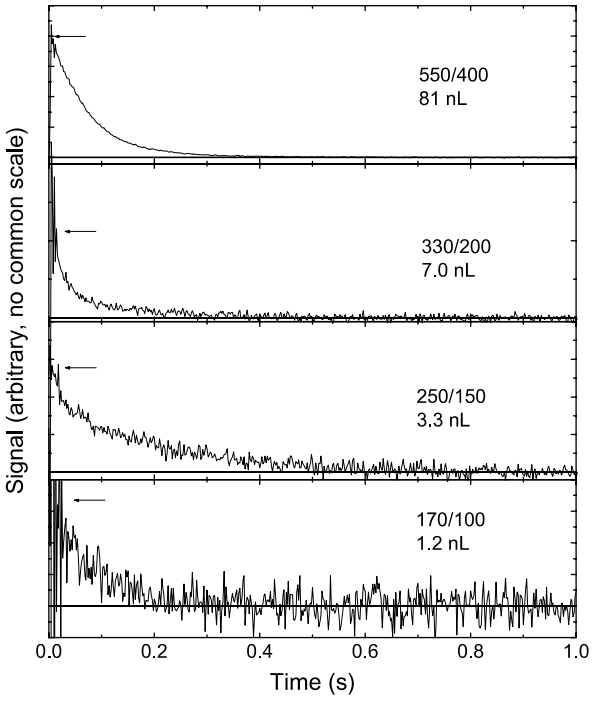

Fig. 2. Single-shot FIDs from each of the four microcoil probes described in Table 1. The complex time domain data were frequency- and phase-shifted so that all of the signal appears in the real-part of the data set, which is plotted here. The zero of the vertical axis is indicated by the horizontal line in each panel. The receiver bandwidth was ±250 Hz for all probes. The SNR value was determined from the extrapolation of the signal-to zero time (as indicated by the arrows) and the rms value of the variations in the baseline.

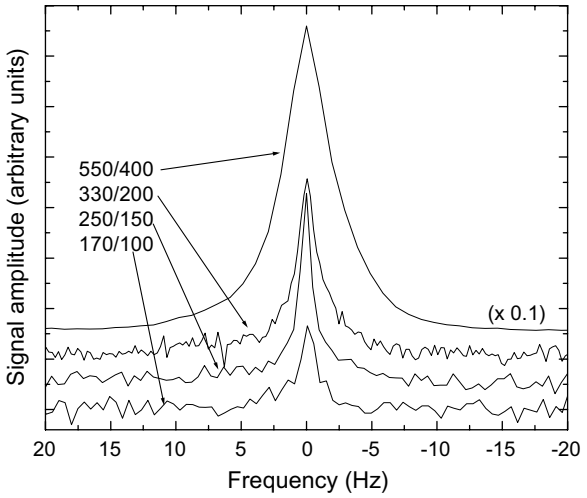

Fig. 3. The best line shapes observed in each of the four microcoil probes described in Table 1. The spectra shown are the Fourier Transforms of single FIDs (i.e., no signal averaging). These were not the same FIDs as shown in Fig. 2. To avoid the influence of distortions of the early-time data due to filter ringing, the FIDs were time shifted before transformation. No zero-filling or apodization methods were applied. The resonance frequency was 44.4 MHz. (The spectrum for the 330/200 probe has higher resolution because twice as many data points were acquired for this probe, giving a two-fold increase in the length of the data acquisition window.)

which have an overall uncertainty of about 0.01 Ω. The right-most column in Table 2 gives the RF power required to produce the 100 μs $\pi/2$ pulse in our experiments. This power was determined by measuring the peak-to-peak voltage of the pulse seen by the probe circuit by routing this pulse to a 50 Ω-terminated oscilloscope. The uncertainty in the measurement comes from the roughly ±10% uncertainty of reading the oscilloscope screen.

4. Discussion

4.1. Comparison to original microcoil results

We have achieved an SNR of 485 ± 50 with the 50 gauge wire-wound 550/400 microcoil using a detection bandwidth of ±250 Hz. To facilitate comparison to our previous focused ion beam (FIB) coil result, we re-analyzed the previous data using the method described above. (Henceforth, we refer to this coil as the "FIB-coil.") The re-analyzed SNR value for the FIB-coil was 38 ± 2 in a detection bandwidth of ±5000 Hz. At this bandwidth, our wire-wound coil should give an SNR of 108 ± 12. To account for the different lengths of the sample volumes, we note that extending our wire-wound coil to the 2.1 mm length of the FIB-coil would enclose 3.24× more volume while increasing the resistance by the same factor. We therefore scale the SNR by $\sqrt{3.24}$ and calculate that a wire-wound coil of the same size as the FIB-coil should yield an SNR of 194 ± 20. Hence, the wire-wound coil achieved a 5-fold (5.1 ± 0.8) improvement in SNR performance over the FIB-coil. The DC resistances of a wire-wound coil that is the same length as the FIB-coil would be 5.22 Ω, compared with the 5.42 Ω of the FIB coil. The pitch of the wire-wound coil is two times finer than the FIB-coil. These two differences account for a factor of two improvement in the SNR. The FIB-coil's probe circuit contained other sources of resistive losses, including the 45 cm quarterwave cable and the long (10 cm) leads between components in the two shielded boxes. These resistances are eliminated in the present design, which helps account for the observed 5-fold improvement in SNR.

In our previous paper [28], we speculated that the narrow line achieved in the FIB-coil was due to the high

Table 2
Measured performance and resistance of microcoils

Probe	Observed SNR (±10%)	Detector bandwidth (Hertz)	SNR/√Hz	Line width (Hertz) (±10%)	Resistance (Ω) (±0.01 Ω)	Power (μW) (±15%)
170/100	10.3	±250	0.46	1.5	0.43	7.6
250/150	46	±250	2.1	1.5	0.44	14
330/200	76	±250	3.4	2.8	0.57	20
550/400	540	±250	24	5	1.61	25

cylindrical symmetry of that coil. Due to the following experiments, we now believe that the main influence on line width is the amount of copper in the coil winding, rather than its detailed geometry.

Before winding the 550/400 coil described in Table 1, we wound a 20 turn coil with 40 gauge enameled copper wire on a 550/400 tube. This coil was 1.5 mm long and contained a sample volume of about 190 nL. The turn–turn spacing was ~80 microns, nearly the same as the FIB-coil, while the volume was about 3/4 of the FIB-coil's sample volume. However, the narrowest line achieved in this 40 gauge probe was 1 ppm, nearly 20× worse than the FIB-coil. Since a narrower line had been achieved over a larger sample volume in the FIB-coil, homogeneity of the background magnetic field could be ruled out as a factor limiting the line width. A series of modifications were made to this 40 gauge probe in order to ascertain the source of the excess line broadening. Guided by the original FIB-coil probe, in which no piece of the probe circuitry or support structure came within 3 mm of the sample volume, new versions of the 40 gauge probe were constructed in which the support structures, electrical circuitry, and fluid handling tubing were all moved well away from the sample volume; no improvement in the line width was observed. The final modification was to replace the 40 gauge with 50 gauge wire. This 50 gauge coil achieved the much smaller line width given in Table 2.

The 550/400 coil wound with 50 gauge wire yielded a line width a factor of two worse than our original FIB-coil result, while the 40 gauge coil was a factor of 10 worse than the 50 gauge coil. These line width differences correlate very well with the cross-sectional areas of the wires in each of the these coils, 4900, 490, and 325 μm^2 for the 40, 50 gauge, and FIB-coils, respectively. (The wire-wound coils were copper. The FIB coil was gold, 3× more diamagnetic than copper, over a very thin chromium layer, which would compensate for the gold to some extent.) Due to the skin-depth effect, only the outer surface of the 40 gauge wire carries current (the "effective area" is 250 μm^2), so most of the copper in that wire is "wasted." This excess copper, although it would not affect the SNR performance of the coil [1], affects the homogeneity of the field in the sample volume. It appears that the presence of copper near the sample volume should be minimized in order to achieve the highest resolution, indicating that wires much larger than the skin depth should be avoided. Of course, susceptibility matching techniques [3,6] may be employed to overcome the distortions of the field due to the wires, but these would complicate our device.

4.2. Performance of smaller coils

As shown in Table 2, the resolution achieved in the three smallest coils is extremely good, approaching 30 ppb using only linear shims. Furthermore, the SNR is high enough that the FID is visible in a single shot, even in the smallest coil's ~1 nL volume. It is clear that our probe circuit design and simple, fast, inexpensive construction methods produce useable NMR detectors. However, we may ask if these detectors are performing optimally.

The SNR value we expect from these coils and probe circuits can be calculated using [29]

$$\mathrm{SNR} = \frac{k_0 (B_1/i) v_s N \gamma \hbar^2 I(I+1)\omega_0^2 / 3 k_B T}{\sqrt{4 k_B T R \Delta f}} \tag{3}$$

Note that reference [1] has an extra factor of $\sqrt{2}$ in the denominator. k_0 is a constant that accounts for geometric effects associated with irregularity of the B_1 field produced by the finite solenoid as well as non-uniform excitation of the spins in the sample volume, v_s. (B_1/i) is the efficiency of the coil in generating B_1, and for a solenoid it has the value $\mu_0 n$, where $\mu_0 = 4\pi \times 10^{-7}$ T m/A and n is the turns per unit length. $N = 6.7 \times 10^{28}/\mathrm{m}^3$ the number density of hydrogen nuclei in our water samples, $\gamma = 2.675 \times 10^8$ radians/s/T is the gyromagnetic ratio for hydrogen nuclei, $I = 1/2$ for hydrogen, $\omega_0 = 2.78 \times 10^8$ radians/s for hydrogen nuclei in our field, $T = 297$ K, R the high frequency resistance of the LC resonant circuit, and Δf the detection bandwidth. k_0 is the only parameter that cannot be measured or calculated easily. It should have a value close to but less than 1.0, and should not differ substantially for our probes because they all have similar coil and sample geometries. Our detectors differ mainly in their sample volumes and resistances.

To calculate the expected SNR, we need to know the RF resistances of each element of the LC resonant circuit. The other parts of the probe, including the matching capacitor, the connections to ground, etc., play a much smaller role in contributing to losses in the circuit because the currents flowing in these sections of the probe are much smaller than in the resonant loop itself. We can calculate the resistances for each element of the resonant circuit by measuring their physical dimensions and considering that current will only flow in the region within a skin depth (10 μm in copper at our frequency) of the surface. For the 50 gauge wire, we measure the DC resistance of the microcoil and its leads; this value is given in Table 2 and repeated in the 2nd column of Table 3 for convenience. We convert this

Table 3
Calculated resistance and SNR performance of microcoil probes

Capillary	R_{DC} (Ω)	Skin depth factor	Proximity factor R_{RF} (Ω)		Auxiliary inductor (Ω)	Total (Ω)	Calculated SNR ($k_0 = 1$)	k_0
170/100	0.43	0.040	0.039	0.45	0.047	0.50	13	0.57
250/150	0.44	0.040	0.044	0.47	0.047	0.52	36	0.92
330/200	0.57	0.040	0.050	0.61	0.047	0.66	67	0.80
550/400	1.61	0.040	0.114	1.82	None	1.82	474	0.81

DC resistance to a calculated RF resistance by using Figs. 2 and 4 in Peck et al. [1]. The RF resistance of the leads is raised by the skin depth effect, the strength of which may be found using Fig. 2 of Peck et al. The factional enhancement to the DC resistance is about 4% for our coils, as shown in the third column of our Table 3. For the wires in a coil, the proximity effect also plays a role. The strength of the proximity effect depends on the number of turns and the coil aspect ratio, and can be calculated using Figs. 2 and 4 in Peck et al. The 4th column in our Table 3 gives the fractional enhancement to the DC resistance due to the proximity effect in each of our coils. The 5th column in our table is the total RF resistance, calculated by applying the enhancement factors to the measured DC resistance, with the proximity effect applied only to the fraction of the wire length in the microcoils. The calculated RF resistance of the auxiliary inductor is given in the 6th column, and the total RF resistance of the LC circuit is given in the 7th. We find that the copper foil and the tuning capacitors contribute negligibly to the resistive losses.

One is faced with a number of definitional questions in linking measurements of absolute SNR to the theory [30,31]. Johnson's measurements were single-channel incoherent measurements of sub-megahertz voltage signals. Our NMR spectrometer processes the signal from the NMR coil to yield two channels of voltage data, each derived from a coherent combining of the NMR voltage signal with a local oscillator. In order to make the most direct connection with the older measurements, we process our two-channel signals by frequency– and phase–shifting them so that the entire signal appears in one of the channels. From this point forward, we treat this single channel as our entire signal, measuring the signal level from its amplitude at zero time and calculating the noise as the standard deviation of the values in the baseline, as described earlier.

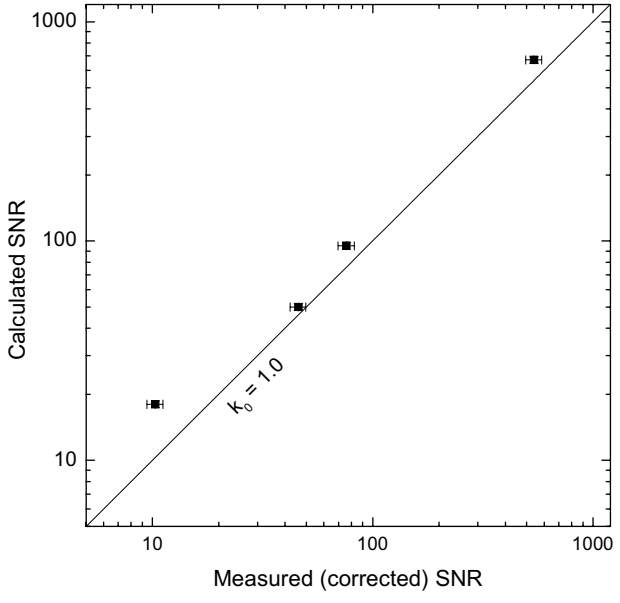

Fig. 4. Calculated SNR versus measured SNR. The calculations were made using Eq. (2) and setting the one unknown parameter, k_0, to unity. The uncertainties in the calculated values come from the 10% uncertainties in the measured DC resistances upon which the calculations are based. The uncertainties in the measured values are estimated from the uncertainty of the extrapolation of the FID data to zero time and the uncertainty in the rms value of the baseline.

A second consideration applies to the definition of the bandwidth Δf. In Nyquist's treatment, the rms voltage noise is white (that is, it has equal powers in every frequency interval Δf). The number 4 in the denominator of Eq. (3) is appropriate for an ideal filter that passes (without any weighting) only frequencies within the bandwidth Δf and excludes all others. Our filters are eighth order, so they closely approximate the ideal filter. For a detector bandwidth of ± 250 Hz, $\Delta f = 500$ Hz.

Table 3 gives the calculated values of SNR assuming $k_0 = 1$. A graphical comparison between the calculated and measured (and corrected) values is given in Fig. 4. The solid line corresponds to complete agreement ($y = x$). We determine experimental values for k_0 by taking the ratio of measured and calculated values. These values of k_0 are given in the last column of Table 3. These values lie between 0.57 and 0.92, with an uncertainty of $\sim$15%. These values are consistent with the homogeneity of the RF magnetic field expected in short solenoids such as ours.

It is also possible to relate the SNR performance of the system to its characteristics in transmit mode [29]. If the current i that gives rise to B_1 flows through the resistance R responsible for the loss, then the power dissipated is $P = 1/2 i_{\text{peak}}^2 R$ and Eq. (3) may be recast in the form:

$$P = \frac{1}{2}\left(\frac{Ak_0 v_s B_1}{\text{SNR}}\right)^2 \tag{4}$$

with $A = 3.27 \times 10^{14}\ \text{watt}^{1/2}\ \text{m}^{-3}\ \text{T}^{-1}$ (for $\Delta f = 500$ Hz). A 100 μs $\pi/2$ pulse corresponds to $B_{\text{RF}} = 0.59\ \text{G} = 5.9 \times 10^{-5}\ \text{T}$. NMR measurements of B_{RF} pick out only half of the linear field, since only the component rotating in the direction of the precession contributes. Hence, $B_1 = 2B_{\text{RF}}$. Using Eq. (4), the sample volumes v_s from Table 1, the measured k_0 values from Table 3, and the measured SNR values from Table 2, we calculate expected RF power requirements of 3.0, 3.1, 4.0, and 10 μW for our four probes. The calculated values, although the same order of magnitude as the measured values given in Table 2, are all lower. We do not currently have a explanation for this.

Table 3 shows that our auxiliary inductor does not decrease the SNR performance unacceptably. We see that in the probes tested, the auxiliary inductor accounts for about 10% of the resistive losses, leading to a 5% decrease in the SNR that might be achieved without it. Removing the inductor therefore will not make a very large improvement in the SNR performance of these probes. However, without the auxiliary inductor, the probe circuit will be much more difficult to construct and operate.

Table 4
Contributions to the resistive losses in the microcoil probe circuits

Capillary (Ω)	Microcoil (Ω)	Leads (Ω)	Total (Ω)	"Measured" total (Ω)	Auxiliary inductor (Ω)
170/100	0.097	0.35	0.44	0.45	0.047
250/150	0.17	0.22	0.39	0.47	0.047
330/200	0.26	0.29	0.55	0.61	0.047
550/400	1.29	0.31	1.60	1.82	None

4.3. Building and testing a better probe

The agreement between the observed and calculated SNR in our first set of probes indicates that we have a good quantitative understanding of the factors contributing to the SNR performance. We now ask if we can improve the SNR.

This is equivalent to asking if there are stray resistances that can be removed. The first set of coils had rather long connections between the microcoils themselves and the remainder of the probe circuit, in order to avoid the homogeneity-degrading effects of large conductors too near the sample. Since these connections are made with the narrow gauge wire, they contribute substantially to the resistance (and hence noise) in our detector, without contributing signal. We have measured the lead lengths of our coils and then used the results of Peck et al. [1] to calculate the separate contributions of the microcoils and the leads to the resistance of the LC circuit. The values are given in the 2nd and 3rd columns of Table 4. The 4th column gives the total calculated RF resistance of the coil and its leads, while the 5th column gives the value of this same quantity that we calculated based on the measured DC resistance (see Table 3). The last column gives the calculated RF resistance of the auxiliary inductor, also from Table 3.

Table 4 indicates that we should build probes with shorter leads in order to achieve higher SNR performance. Shortening the leads requires that we bring larger conductors closer to the sample volume. Given our experience with the 40 gauge wire and the 550/400 coil, we expect that we will eventually degrade the resolution as larger amounts of copper are placed closer to the sample volume. A compromise between resolution and SNR, informed by the requirements of the measurements to be performed, will govern the optimization of the probe circuit design. Work toward finding the best compromise is underway.

5. Conclusions

We have shown that very small microcoils can readily be operated as NMR detectors in the low magnetic fields of permanent magnets, a new size and frequency regime for miniaturized NMR detectors. The close agreement in the measured SNR and the values calculated based on a detailed analysis of the sources of resistive losses in our NMR probes indicate that the very simple construction methods we employ yield nearly optimal probes. In particular, the SNR performance confirms that our novel auxiliary "tuning" inductor does not degrade SNR performance. The detailed analysis of the resistive losses also points the way toward available improvements in SNR performance: reduction of the leads connecting the microcoil to the remainder of the probe circuit. However, reduction of these lead lengths must respect the fact that bringing more metal closer to the sample volume can readily degrade the field homogeneity. The understanding of probe performance will also guide the full miniaturization of the probe circuit, necessary to fit the NMR detector coil into our 5 mm gap permanent magnet.

Acknowledgment

Helpful conversations with Mark Conradi and Eiichi Fukushima are gratefully acknowledged. Mladen Barbic motivated us to consider simpler coil manufacturing techniques and provided valuable consultations.

References

[1] T.L. Peck, R.L. Magin, P.C. Lauterbur, Design and analysis of microcoils for NMR microscopy, J. Magn. Reson. B 108 (1995) 114–124.
[2] D.L. Olsen, T.L. Peck, A.G. Webb, R.L. Magin, J.V. Sweedler, High-resolution microcoil ^{1}H-NMR for mass-limited, nanoliter-volume samples, Science 270 (1995) 1967.
[3] A.G. Webb, S.C. Grant, Signal-to-noise and magnetic susceptibility trade-offs in solenoidal microcoils for NMR, J. Magn. Reson. B 113 (1996) 83–87.
[4] J.A. Rogers, R.J. Jackman, G.M. Whitesides, D.L. Olson, J.V. Sweedler, Using microcontact printing to fabricate microcoils on capillaries for high resolution proton nuclear magnetic resonance on nanoliter volumes, Appl. Phys. Lett. 70 (1997) 2464–2466.
[5] J.E. Stocker, T.L. Peck, A.G. Webb, M. Feng, R.L. Magin, Nanoliter volume high-resolution NMR microspectroscopv using a 60-um planer microcoil, IEEE Trans. Biomed. Eng. 44 (1997) 1122–1127.
[6] B. Behnia, A.G. Webb, Limited-sample NMR using solenoidal microcoils, perfluorocarbon plugs, and capillary spinning, Anal. Chem. 70 (1998) 5326–5331.
[7] R. Subramanian, M.M. Lam, A.G. Webb, RF microcoil design for practical NMR of mass-limited samples, J. Magn. Reson. 133 (1998) 227–231.
[8] D.L. Olson, M.E. Lacey, J.V. Sweedler, High-resolution microcoil NMR for analysis of mass-limited, nanoliter samples, Anal. Chem. 70 (1998) 645–650.
[9] V. Malba, R. Maxwell, L.B. Evans, A.F. Bernhardt, M. Cosman, K. Yan, Laser-lathe lithography—a novel method for manufacturing nuclear magnetic resonance microcoils, Biomed. Microdev. 5 (2003) 21–27.
[10] D. Djukovic, S. Liu, I. Henry, B. Tobias, D. Rafferty, Signal enhancement in HPLC/microcoil NMR using automated column trapping, Anal. Chem. 78 (2006) 7154–7160.

[11] N. Wu, T.L. Peck, A.G. Webb, R.L. Magin, J.V. Sweedler, ^{1}H-NMR spectroscopy on the nanoliter scale for static and on-line measurements, Anal. Chem. 66 (1994) 3849.
[12] J.D. Trumbull, I.K. Glasgow, D.J. Beebe, R.L. Magin, IEEE Trans. Biomed. Eng. 47 (2000) 3.
[13] C. Massin, F. Vincent, A. Homsy, K. Ehrmann, G. Boero, P.-A. Besse, A. Daridon, E. Verpoorte, N.F. de Rooij, R.S. Popovic, Planar microcoil-based microfluidic NMR probes, J. Magn. Reson. 164 (2003) 242–255.
[14] B. Sorli, J.F. Chateaux, M. Pitaval, H. Chahboune, B. Favre, A. Briguet, P. Morin, Micro-spectrometer for NMR: analysis of small quantities in vitro, Meas. Sci. Technol. 15 (2004) 877–880.
[15] D.A. Seeber, J.H. Hoftiezer, W.B. Daniel, M.A. Rutgers, C.H. Pennington, Triaxial magnetic field gradient system for microcoil magnetic resonance imaging, Rev. Sci. Inst. 71 (2000) 4263–4272.
[16] S.C. Grant, N.R. Aiken, H.D. Plant, S. Gibbs, T.H. Mareci, A.G. Webb, S.J. Blackband, NMR spectroscopy of single neurons, Magn. Reson. Med. 44 (2000) 19–22.
[17] D.A. Seeber, R.L. Cooper, L. Ciobanu, C.H. Pennington, Design and testing of high sensitivity microreceiver coil apparatus for nuclear magnetic resonance and imaging, Rev. Sci. Inst. 72 (2001) 2171–2179.
[18] S.C. Grant, L.A. Murphy, R.L. Magin, G. Friedman, Analysis of multilayer radio frequency microcoils for nuclear magnetic resonance spectroscopy, IEEE Trans. Magn. 37 (2001) 2989–2998.
[19] L. Ciobanu, C.H. Pennington, 3D micron-scale MRI of single biological cells, Solid State Nucl. Magn. Reson. 25 (2004) 138–141.
[20] H. Wensink, D.C. Hermes, A. van den Berg, High signal-to-noise-ratio in low-field NMR on a chip: simulations and experimental results, 17th IEEE MEMS (2004) 407–410.
[21] G. Moresi, R.L. Magin, Miniature permanent magnet for table-top NMR, Concept. Magn. Res. 19B (2003) 35–43.
[22] S. Anferova, V. Anferov, D.G. Rata, B. Blumich, J. Arnold, C. Clauser, P. Blumler, H. Raich, A mobile NMR device for measurements of porosity and pore size distributions of drilled core samples, Concept. Magn. Reson. 23B (2004) 26–32.
[23] W.H. Chang, J.H. Chen, L.P. Hwang, Single-sided mobile NMR with a Halbach magnet, Magn. Reson. Imag. 24 (2006) 1095–1102.
[24] A.G. Goloshevsky, J.H. Walton, M.V. Shutov, J.S. de Ropp, S.D. Collins, M.J. McCarthy, Development of low field nuclear magnetic resonance microcoils, Rev. Sci. Inst. 76 (2005) 024101.
[25] A.G. Goloshevsky, J.H. Walton, M.V. Shutov, J.S. de Ropp, Integration of biaxial planar gradient coils and an RF microcoil for NMR flow imaging, Meas. Sci. Technol. 16 (2005) 505–512.
[26] K. Halbach, Design of permanent multipole magnets with oriented rare earth cobalt material, Nucl. Instrum. Method. 169 (1980) 1–10.
[27] E. Fukushima, S.B.W. Roeder, Experimental Pulse NMR, Addison-Wesley, New York, 1981.
[28] L.O. Sillerud, A.F. McDowell, N.L. Adolphi, R.E. Serda, D.P. Adams, M.J. Vasile, T.M. Alam, ^{1}H-NMR detection of superparamagnetic nanoparticles at 1 T using a microcoil and novel tuning circuit, J. Magn. Reson. 181 (2006) 181–190.
[29] D.I. Hoult, R.E. Richards, The signal-to-noise ratio of the nuclear magnetic resonance experiment, J. Magn. Reson. 24 (1976) 71–85.
[30] J.B. Johnson, Thermal agitation of electricity in conductors, Phys. Rev. 32 (1928) 97–109.
[31] H. Nyquist, Thermal agitation of electric charge in conductors, Phys. Rev. 32 (1928) 110–113.